NO Monomers on MgO Powders and Thin Films

Cristiana Di Valentin,[†] Gianfranco Pacchioni,*[,†] Mario Chiesa,[‡] Elio Giamello,[‡] Stéphane Abbet,[§] and Ueli Heiz[||]

Dipartimento di Scienza dei Materiali, Università di Milano-Bicocca, and Istituto Nazionale per la Fisica della Materia, via R. Cozzi, 53 - I-20125 Milano, Italy, Dipartimento di Chimica IFM, Univeristà di Torino, and Istituto Nazionale per la Fisica della Materia, via P. Giuria 5, I-10125 Torino, Italy, Institut de Physique de la Matière Condensée, Université de Lausanne, CH-1015 Lausanne, Switzerland, and Institute of Surface Chemistry and Catalysis, University of Ulm, D-89069 Ulm, Germany

Received: July 18, 2001; In Final Form: September 27, 2001

The interaction of nitric oxide with the surface of MgO at low temperature has been studied experimentally and theoretically. High-surface-area polycrystalline MgO prepared by chemical vapor deposition has been exposed to both ^{14}NO and ^{15}NO and the corresponding adsorption complexes have been monitored by means of electron paramagentic resonance (EPR) spectra. MgO(100) thin films grown on Mo(100) in UHV conditions have been exposed to ^{15}NO and the adsorption products have been investigated by thermal desorption (TDS) and Fourier transform infrared (FTIR) spectroscopies. The structure and properties of NO/MgO(100) have been studied by cluster model density functional theory (DFT) calculations. The EPR data show that only 0.5% of the total NO deposited is in a paramagnetic state; out of the paramagnetic species, 98% are physisorbed and only 2% are chemisorbed. This is explained with the fact that on the terrace sites NO monomers interact very weakly and prefer to form dimers, $(NO)_2$. Only at defect sites (low-coordinated cations) the interaction of NO monomers with the MgO surface is stronger and prevents the formation of the diamagnetic dimers. A small minority of chemisorbed species is formed only at low coordinated anions (steps, edges, or corners) or oxygen vacancies.

1. Introduction

The study of the interaction of NO with alkaline earth metal oxide surfaces is of interest for the development of novel catalysts active in the reduction of nitrogen oxides from car exhausts. In fact, NO adsorbed on the surface of MgO, CaO, or other oxides in this series gives rise to a rich and complex chemistry which is still under investigation. The various oxides exhibit some similarities but also considerable differences which can be explained with their different electronic structure, and in particular with the different basicity of their surface sites. Another point which has drawn a lot of attention is the role of morphological defects, vacancies, and impurity atoms in determining the chemistry of nitrogen oxides on these oxides. MgO is by far the most studied system.[1] On a flat, defect-free MgO(100) single-crystal surface NO interacts very weakly. Thermal desorption spectra in UHV show a desorption peak between 75 and 84 K, depending on the coverage.[2,3] A small feature at 100 K has been attributed to NO desorption from defect sites. Assuming a frequency factor of 10^{13}, adsorption energies calculated via the Redhead equation indicate a binding energy for NO on the terrace sites of MgO of 0.22 eV only.[2,3] Thus, single-crystal MgO exhibits no chemical activity at all. This is different from the reactivity observed on MgO thin films grown in UHV on a Mo(100) substrate. This is due to the presence of defects which result in new spectroscopic features in the gap of the material.[4] NO adsorption on defective films shows that NO dissociation occurs at 90 K with consequent formation of N_2O.[4]

A spectroscopic study of NO adsorption on polycrystalline MgO at 77 K and RT has been reported by Escalona-Platero et al.[5,6] The infrared (IR) spectra show two regions, one at 1800−1900 cm^{-1} and one between 1100 and 1400 cm^{-1}, which have been attributed to the formation of $(NO)_2$ dimers and $(NO_2)^{2-}$ species, respectively. In one of these studies the existence of a monomeric nitrosylic species has been excluded even at low coverages, in favor of the more stable dimeric form.[5] This result contrasts in part with the electron paramagnetic resonance (EPR) study of Lunsford[7] and Zhang et al.[8] who showed the formation of two paramagnetic species when NO is adsorbed on high-surface-area MgO. The first radical is identified as the $(NO_2)^{2-}$ complex which is stable at RT, while the other radical is identified as a NO molecule perturbed by the surface electric field.[7]

Not surprisingly, the abundant set of experimental data has stimulated a corresponding to theoretical activity. Lu et al.[9,10] have used cluster models to study the interaction of NO on MgO and the formation of $(NO)_2$, $(NO_2)^{2-}$, and $(N_2O_3)^{2-}$. They also computed the IR spectra of *cis*-$(NO)_2$, $(NO_2)^{2-}$, and $(N_2O_3)^{2-}$. Yanagisawa et al.[11] have studied the IR properties of chemically reacted NO molecules, i.e., the spectral region corresponding to $(NO_2)^{2-}$ complexes. Rodriguez et al.[12,13] have reported and analyzed the ultraviolet photoemission spectra (UPS) of NO adsorbed on pure and Ni-doped MgO, showing the importance

* Author to whom correspondence should be addressed at Dipartimento di Scienza dei Materiali, Università di Milano-Bicocca, via R. Cozzi, 53-20125 Milano, Italy. Tel: +39-02-6448 5219. Fax: +39-02-6448 5403. E-mail: gianfranco.pacchioni@unimib.it.

[†] Dipartimento di Scienza dei Materiali, Università di Milano-Bicocca and Istituto Nazionale per la Fisica della Materia.

[‡] Dipartimento di Chimica IFM, Università di Torino, and Istituto Nazionale per la Fisica della Materia.

[§] Institut de Physique de la Matière Condensée, Université de Lausanne.

[||] Institute of Surface Chemistry and Catalysis, University of Ulm.

10.1021/jp0127770 CCC: $22.00
Published on Web 01/30/2002

of the oxygen vacancies at the MgO surface to enhance the NO binding. The role of these defects has been discussed also by Snis and Panas in a quantum-chemical study of NO on CaO.[14]

From the existing literature it appears that several species can form on the MgO surface upon adsorption of the NO radical. This depends on NO coverage, temperature, and also on sample preparation and number of defects or impurities present on the surface. In this study we reconsider the initial phases of NO deposition using a combined experimental−theoretical approach. The chemical reactivity of the molecule, with formation of N_2O and other products, will be the subject of future work.[15] Two completely different forms of the MgO substrate have been used: a high-surface-area polycrystalline form obtained by chemical vapor deposition (CVD), and a MgO ultrathin film grown in UHV on a Mo(100) substrate. The properties of adsorbed NO have been analyzed by means of EPR, TDS, and IR measurements. The experimental data are complemented and compared with embedded cluster model calculations. From the comparison of measured and computed properties we believe that a deeper understanding of the interaction of molecular NO with the surface of MgO has been obtained.

2. Methods

2.1. MgO Polycrystals by CVD. The experiments on polycrystalline MgO were carried out on two types of samples. The first type was prepared by chemical vapor deposition (CVD) in a flow system[16] and kindly supplied by Prof. Erich Knözinger (Institut für Physikalische Chemie Technische Universität Wien). Samples were activated at 1173 K under dynamic vacuum in order to obtain a totally dehydroxylated surface. The resulting surface area after this treatment was $\approx$320 $m^2\ g^{-1}$. Analogous results were obtained by using the second type of solid which was high-surface-area (HSA) MgO produced by thermal decomposition of $Mg(OH)_2$ under dynamic vacuum at 523 K for 16 h, and then dehydrated at 1073 K. In this case the powder has a surface area of 200 $m^2\ g^{-1}$.

High purity ^{14}NO (Matheson) and ^{15}NO (Icon Service) gases were purified before admission by the freeze−pump−thaw technique. X-band EPR spectra were recorded at 298 K and 77 K on a Bruker EMX spectrometer equipped with a cylindrical cavity. The EPR computer simulations were obtained using a program derived from the SIM14S [QCPE] and adapted for the personal computer.

2.2. MgO(100) Thin Films. The MgO(100) films are grown on Mo(100) by evaporating pure metallic magnesium at an oxygen pressure of 5×10^{-7} mbar and are subsequently annealed to 840 K. Auger electron spectroscopy (AES) measurements show a one-to-one stoichiometry of the films and the absence of any impurities.[17] Typical thicknesses were about 10 monolayers, as determined by AES peak intensities and by X-ray photoemission (XPS) using the intensity attenuation of the Mo 3d core level with increasing film coverage.[18]

Low energy electron diffraction (LEED) taken of a MgO film after a short annealing shows a sharp (1×1) pattern.[18] Multiple phonon losses in the high-resolution energy loss spectrum (HREELS), the characteristic UPS from the O 2p valence band, and electron energy loss spectra (EELS) with the characteristic loss at about 6 eV,[18] indicate a well-ordered MgO(100) single-crystal surface in good agreement with previous studies.[19−23]

Although these MgO(100) films reveal properties similar to those observed for the corresponding three-dimensional solids, they expose, depending on the Mg evaporation rate, O_2 background pressure, and annealing temperature, a reproducible density of defects on their surface. These defects are characterized by the adsorption properties of small molecules. For CO chemisorption on MgO(100) it was concluded from highly accurate first-principle theoretical model calculations[24] that the relatively strong chemisorption energy coupled with an unusual blue shift of the CO frequency in CO/MgO(100)/Mo(100) reported experimentally[25] cannot correspond to chemisorption on regular, unperturbed five-coordinated sites as claimed.[2,3] Rather, it was suggested that the unusually strong interaction should be connected with extended defects (steps, kinks) on the oxide film. In addition to the extended defect sites, oxygen vacancies (F-centers) could be detected.[26] The existence of F-centers is deduced from the good agreement of experimental and theoretical binding energies and vibrational frequencies of CO adsorbed to single Pd atoms trapped on the point defects. STM measurements of a 2 ML MgO/Ag(001) thin film, epitaxially grown at 500 K, also point to the existence of F-centers.[27,28]

The in-situ prepared films were then exposed to 5 Langmuir of ^{15}NO (Isotec) with a calibrated molecular beam doser. The adsorbed nitric oxide was then characterized by using thermal desorption spectroscopy (TDS) and Fourier transform infrared (FTIR) spectroscopy. For the TDS experiments a heating rate of 2K/s was used and the desorbing molecules were detected with a differentially pumped mass spectrometer (Balzers QMS 420) after electron impact (70 eV) ionization. The infrared spectra were measured in single reflection mode where the infrared beam is focused at grazing angle (85°) onto the sample. The reflected beam was detected by a narrow band MCT detector. 512 interferograms were averaged and no baseline correction and smoothing of the spectra were performed.

2.3. Computational Details. The interaction of NO with regular and low-coordinated sites of the MgO surface has been studied by means of cluster models. This approach has been widely used to study the adsorption and reaction of molecules with oxide surfaces and it properly describes the physics of local surface processes.[29,30] Due to the highly ionic nature of MgO, the truncation of the crystal lattice implies the use of an external field to represent the long-range Coulomb potential. All the selected model clusters have been embedded in a large array of point charges, PC $\pm$ 2, to reproduce the correct Madelung potential at the adsorption site.[31] Previous studies[32−34] have demonstrated that the use of PCs for embedding can significantly affect the calculated adsorption properties when the positive PCs are nearest neighbors to the highly polarizable oxygen anions of the clusters. This problem can be eliminated by using an effective core potential (ECP) instead of positive PCs at the cluster borders.[32,33] Various clusters have been used to describe the different sites on the MgO surface. They have been constructed trying to fulfill some general requirements: (1) at least first and second neighbors to the adsorption site must be included; in some cases, there are two possible sites where the NO molecule can bind and first and second neighbors to the two sites are present; (2) the Mg_nO_n clusters are stoichiometric, i.e., have the same number of anions and cations; (3) the ions, ECPs and PCs taken together, are electrically neutral. These criteria give rise to clusters of various size, but previous experience has shown that the results are generally not dependent on the cluster size.

The calculations were performed using both Hartree−Fock (HF) and gradient-corrected density functional theory (DFT) methods. In DFT we have used the Becke's three parameters hybrid exchange functional[37] in combination with the correlation functional of Lee, Yang and Parr[38] (B3LYP). Gaussian-type atomic orbital basis sets have been used to construct the Kohn−

Sham orbitals. The basis set adopted for the NO molecule is 6-31+G* while that for the O^{2-} and Mg^{2+} active ions and their first neighbors is 6-31G*.[39] The rest of the ions of the MgO cluster have been treated with a 6-31G basis set. The hyperfine constants have been determined at the optimal geometry using the EPR-II[40] basis set on O and N atoms. The EPR-II basis set reproduces accurately the hyperfine coupling constants (hfc) for some second-row atoms.

The geometry of adsorbed NO has been fully optimized by means of analytical gradients. In the MgO clusters the O and the Mg ions first neighbors to the adsorbing site (if not directly in contact with point charges) were free to move, while the positions of all the other atoms were kept fixed at bulk values. All the adsorption energies, D_e, have been corrected by the basis set superposition error (BSSE) by applying the standard counterpoise method.[41] A full vibrational analysis, based on second derivatives of the total energy, has been performed to compute the harmonic frequencies of NO adsorbed on the various sites of MgO.

The hyperfine interactions of the electron spin with the nuclear spin of the paramagnetic NO molecule, ^{14}N and ^{17}O nuclides, have been determined. The hyperfine spin-Hamiltonian, $H_{hfc} = \mathbf{S}\cdot\mathbf{A}\cdot\mathbf{I}$, for each is given in terms of the hyperfine matrix **A** which describes the coupling of the electron with the nuclear spin.[42] The components of **A** can be represented as

$$\mathbf{A} = \begin{bmatrix} A_1 & 0 & 0 \\ 0 & A_2 & 0 \\ 0 & 0 & A_3 \end{bmatrix} = a_{iso}\mathbf{U} + \begin{bmatrix} B_1 & 0 & 0 \\ 0 & B_2 & 0 \\ 0 & 0 & B_3 \end{bmatrix} \quad (1)$$

where **U** is the unit matrix and B are the components of a usually traceless matrix of the type: $[-B\ 2B\ -B]$. The isotropic part, a_{iso}, of each coupling constant is related to the spin density at the nucleus (the Fermi contact term):

$$a_{iso} = (2\mu_o/3)\, g_N\, \beta_N\, g_e\, \mu_B\, \langle \rho^s \rangle \quad (2)$$

where μ_o is the permeability of free space, g_N is the nuclear g-factor, g_e is the electronic g-factor for the site under consideration, β_N and μ_b are the nuclear and Bohr magnetons, respectively, and $\langle \rho^s \rangle$ is the expectation value at the nucleus of the spin-density operator. In one-electron systems, $\langle \rho^s \rangle = |\Psi^s(0)|^2$. The anisotropic traceless tensor **B** results from the dipolar interaction:

$$B_{ij} = (\mu_o/4\pi)\, g_N\, \beta_N\, g_e\, \mu_B \int (3x_i x_j/r^5 - \delta_{ij}/r^3)\, |\Psi(r)|^2\, dV \quad (3)$$

The calculations have been performed using the Gaussian-98[43] program package.

3. Results

3.1. Polycrystalline MgO. *3.1.1. The EPR Spectra of Adsorbed NO.* The interaction of nitric oxide with the surface of fully dehydrated MgO was studied by EPR in order to identify paramagnetic species derived by interaction of the surface with the NO molecule. The experimental results on polycrystalline MgO were very well reproducible and independent of the type of material used (CVD and ex-hydroxide). In two papers published in 1985 Zecchina and co-workers,[4,5] on the basis of an IR investigation of the NO−MgO interaction at 77 K, suggested the formation at the surface of three main species, i.e., $(NO)_2$ dimers, nitrites $(NO_2)^-$, and hyponitrite $(N_2O_2)^{2-}$ anions. No monomeric neutral NO species was assigned by these authors whereas the formation of such a molecular species was proposed by Lunsford in an earlier paper[7] on the basis of EPR spectroscopic evidence. The results reported in the following confirm Lunsford's findings but provide more resolved spectra allowing a deeper insight in the various sites capable of NO coordination. Two types of species are actually observed by EPR when NO is adsorbed at the surface of dehydrated MgO. The first one is a rather strongly bound species that forms at room temperature and does not desorb upon evacuation at the same temperature. This species, hereafter indicated as chemisorbed species, exhibits a weak and poorly resolved EPR spectrum since it is formed in very small amounts at the surface, Figure 1. The same species, also described in ref 7, was assigned in that paper to a surface $(NO_2)^{2-}$ radical ion on the basis of the g values and of the rather large nitrogen hyperfine coupling constant (^{14}N has a spin nuclear value $I = 1$). The whole set of parameters for this chemisorbed species is reported in Table 1. To observe the EPR spectrum of this species at low temperature (77 K, Figure 1) it is necessary to completely remove NO from the gas phase. In fact, if the temperature is lowered in the presence of NO (about 10 Torr) the spectrum of $(NO_2)^{2-}$ is covered by the onset of a new much more intense spectrum which is reported in Figure 2a together with its computer simulation, Figure 2b. The spectrum, whose main feature is a N hyperfine triplet centered at about $g = 1.99$, exhibits also three different lines at a higher field ($g = 1.9610$, $g = 1.9188$, $g = 1.8900$) which are independent one from the other. Each of these high field lines is split in three components by N hyperfine interaction but the splitting is clearly appreciable only on the third line ($g = 1.8900$). The spectrum in Figure 2 has therefore been interpreted in terms of three distinct NO molecular species weakly adsorbed at the surface, differing essentially in the higher field (g_{zz}) value, Table 1. This interpretation is fully supported by the computer simulation (Figure 2b). The experimental spectrum was simulated on the basis of the following spin-Hamiltonian:

Figure 1. EPR spectrum of chemisorbed ^{14}NO, $(NO_2)^{2-}$, taken at 77 K after removal of physisorbed and gas-phase NO.

$$\mathbf{H} = \mu_B \mathbf{B}\mathbf{g}\mathbf{S} + \mathbf{I}\mathbf{A}\mathbf{S} \quad (4)$$

introducing in the simulation the parameters reported in Table 1 for the three molecular species, NO(a), NO(b), NO(c). The accuracy in the determination of the g_{xx} and g_{yy} component is higher for the species NO(a) than for the other two species whose lines are substantially covered by the more intense line of species a. However, the quality of the assignment is rather good as indicated by the spectrum recorded using ^{15}NO ($I(^{15}N) = 1/2$) instead of ^{14}NO, Figure 3. In this case each hyperfine triplet is substituted by a doublet (see for instance the component

TABLE 1: Spin-Hamiltonian Values for Paramagnetic NO Species Adsorbed on MgO

	g values				A (^{14}N) (G)			A (^{15}N) (G)			
species	g_1	g_2	g_3	Δ (eV)	A_1	A_2	A_3	A_1	A_2	A_3	Ab[a] %
$(NO_2)^{2-}$	2.0100 ± 0.0020	2.0044 ± 0.0005	2.0078 ± 0.0020		unres	40.6	unres	unres	56.8	unres	2
species	g_{xx}	g_{yy}	g_{zz}	Δ (eV)	A_{xx}	A_{yy}	A_{zz}	A_{xx}	A_{yy}	A_{zz}	Ab[a] %
NO (a)	1.9948 ± 0.0005	1.998 ± 0.001	1.8900 ± 0.0002	0.075	32	2.57	8.86	44.8	3.60	12.4	55
NO (b)	1.995 ± 0.001	1.997 ± 0.002	1.9188 ± 0.0002	0.1	32.5	unres	unres	45.5	unres	unres	32
NO (c)	1.995 ± 0.002	1.996 ± 0.002	1.9610 ± 0.0002	0.2	32.6	unres	unres	45.6	unres	unres	11

[a] Relative abundance with respect to the total number of paramagnetic species.

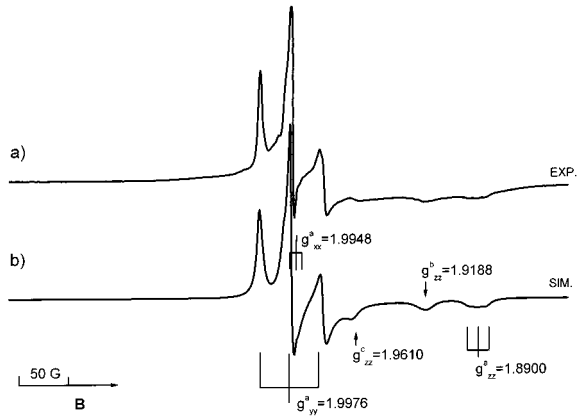

Figure 2. EPR spectrum of physisorbed ^{14}NO at 77 K. (a) Experimental spectrum; (b) simulated spectrum.

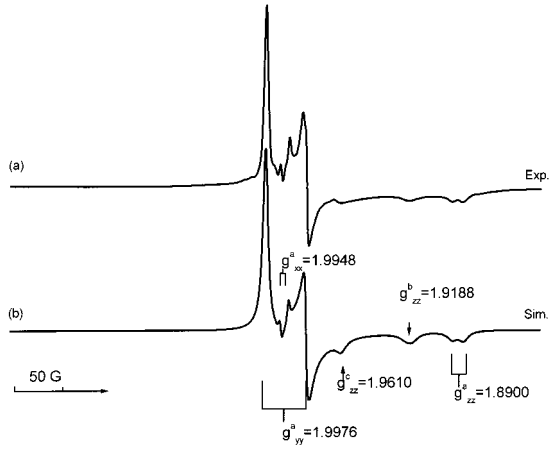

Figure 3. EPR spectrum of physisorbed ^{15}NO at 77 K. (a) Experimental spectrum; (b) simulated spectrum.

at $g = 1.8900$). The simulation in Figure 3b of the spectrum of adsorbed ^{15}NO has been derived employing the same parameters used for the simulation shown in Figure 2b, just introducing the new spin nuclear value (1/2) and scaling the hyperfine coupling of the expected value dictated by the ratio of the two g nuclear factors of ^{14}N and ^{15}N, $g_N(^{15}N)/g_N(^{14}N) = 1.41$.

The structure of each signal in the spectra in Figures 2 and 3 ($g_x \approx g_y > g_z$, $A_{yy} > A_{zz} > A_{xx}$) is in agreement with what is expected for an 11 valence electrons diatomic π radical like NO. In such cases the z direction is assumed to be that of the internuclear axis. The three species (whose relative abundance evaluated by simulation of the spectra is also reported in Table 1) are weakly adsorbed at the surface (physisorbed species) as their spectrum disappears upon temperature increase to room temperature. The number of species remains the same even lowering the temperature down to 4 K. Comparing the intensities of the EPR spectra recorded for adsorption of NO on bare MgO and on MgO containing a controlled amount of Ni^{2+} ions[44] the coverage of paramagnetic NO monomers on MgO was evaluated to be about 0.5% of the whole surface.

SCHEME 1

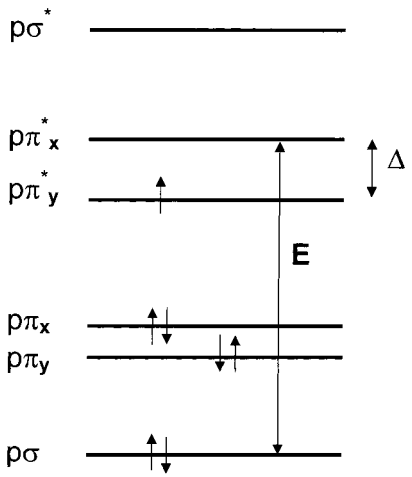

3.1.2. The g-Tensor of Physisorbed NO and the Δ Orbital Splitting Parameter. The electronic configuration of NO is that of a 11 electron diatomic π radical ($^2\Pi_{1/2}$ state) characterized by the presence of a single unpaired electron in the π antibonding orbitals. The physisorption interaction between the surface of MgO and NO illustrated before is based on a weak polarization of the molecule produced by the electric field present at the surface of the ionic solid in correspondence of three specific adsorption sites. This causes a perturbation on the NO molecular orbitals and a consequent split of the two π^* levels (Scheme 1 reports the energy levels of the adsorbed NO species). The described electronic configuration leads to an orthorhombic g tensor whose elements were obtained by Brailsford et al.[45] adapting the equations originally derived by Känzig and Cohen[46] for the $^2\Pi_{3/2}$ state. A simplified form of these equations is as follows:

$$g_{zz} = g_e - 2l\sin 2\alpha \quad (5)$$

$$g_{yy} = g_e \cos 2\alpha + (\lambda/E)(1 + \cos 2\alpha + \sin 2\alpha) \quad (6)$$

$$g_{xx} = g_e \cos 2\alpha + (\lambda/E)(\cos 2\alpha - \sin 2\alpha - 1) \quad (7)$$

where λ is the spin−orbit coupling constant, E and Δ are the energy differences shown in Scheme 1, while tan 2α is defined as λ/Δ. The term l is defined as $l = \lambda/\lambda_0$, i.e., the ratio between the actual value assumed by the spin−orbit coupling constant in the investigated radical and the atomic reference value. It follows from the above equations that $g_{yy} > g_{xx} > g_{zz}$, and an important shift from g_e is expected for one component only, g_{zz}, the component corresponding to the direction of the internuclear axis, as indeed observed in our spectra. The parameter that mainly determines this shift is the energy splitting

TABLE 2: Molecular Parameters and Spin Density Analysis for the Physisorbed NO(a) Species

	parameters (eV)			Δg_{ii}[a]			spin density on N			
	λ	Δ	E	x	y	z	ρ_{2p_x}	ρ_{2p_y}	ρ_{2s}	ρ_N (tot)
NO[a]	0.0067	0.075	4.18	3×10^{-10}	5×10^{-9}	1×10^{-10}	0.106	0.686	0.011	0.803

[a] The parameter Δg_{ii} [$\Delta g_{ii} = g_{ii}$ (calc) $- g_{ii}$(exp)] measures the quality of the fit. g_{ii} (calc) are the g values derived introducing the calculated parameters in eqs 5−7. g_{ii}(exp) are the experimental values of Table 1.

Δ (Scheme 1) which is, in turn, a sort of fingerprint of the ability of the adsorption site to split the π antibonding orbitals. At first order, in fact, eq 5 reduces to

$$g_{zz} = g_e - 2\lambda/\Delta \tag{8}$$

We have calculated the parameters λ, Δ, E for the NO(a) species, Table 2, by fitting the experimental g-tensor to the above equations (5−7) using a routine contained in the Mathcad package. The quality of the fit is measured by the Δg_{ii} parameter reported in Table 2. We have assumed $\lambda_0 = 0.01071$ eV. This value is the average of the two corresponding atomic values λ_0(N) and λ_0(O) weighted on the N and O character (0.8 and 0.2, respectively) of the SOMO (singly occupied molecular orbital) as calculated from the hyperfine tensor (see the following section). The accuracy in the determination of the g values for species b and c, Table 1, was not good enough to allow the use of the extremely sensitive system of eqs 5−7 for these two species. To calculate the Δ value (which is, also in view of the theoretical calculations reported in this paper, the most important of the three parameters) for species b and c we have thus used eq 5 only, introducing the λ value calculated for species a (0.067 eV). Due to the weak interaction between all the NO species and the surface this assumption seems quite reasonable. The Δ values derived from this optimization are listed in Table 1 and are a measure of the extent of the interaction between the NO molecule and the electrostatic field of the various surface sites. As expected, due to the weak NO−surface interaction, the Δ values for the three NO species are rather small, ranging between 0.075 and 0.2 eV.

3.1.3. The ^{14}N Hyperfine Tensor and the Spin Density on the Nitrogen Atom. The hyperfine structure resolution of spectra in Figures 1 and 2, though rather satisfactory, is not complete as, for two of the three NO species, the value of the relatively small A_{zz} splitting is undetectable. We will limit ourselves to the analysis of the NO(a) species for which the whole hyperfine tensor is resolved. The analysis of the hyperfine tensor requires knowledge of the sign of the nitrogen coupling constants that cannot be derived from powder spectra. However, also based on the theoretical calculations reported in the following, the only reasonable choice is that $A_{yy} > 0$, while A_{xx} and $A_{zz} < 0$ since all other combinations lead to unacceptable results. This choice of signs implies, as expected, that $a_{iso} > 0$. The largest value of the hyperfine tensor corresponds to the direction (y). The experimental **B** tensor derived according to eq 1 is not exactly axial but can be easily decomposed into two traceless components ($2a$, $-a$, $-a$) and ($-b$, $2b$,$-b$) as follows:

$$^{NO}A = \begin{vmatrix} -2.57 & & \\ & 32.0 & \\ & & -8.86 \end{vmatrix} = 6.86 + \begin{vmatrix} 4.20 & & \\ & -2.10 & \\ & & -2.10 \end{vmatrix} + \begin{vmatrix} -13.6 & & \\ & 27.2 & \\ & & -13.6 \end{vmatrix} \tag{9}$$

This indicates that although the unpaired electron is mainly confined in one of the two π levels (π_y), a partial admixture of the π_x orbital occurs via spin−orbit interactions. Using the reported atomic value[42] of the dipolar ^{14}N constant $B^o = 4/5 g_N \beta_n \langle r^{-3} \rangle_{2p} = 39.62$ G the spin density on the nitrogen 2p orbitals can be calculated by direct comparison of the experimental $2a$ and $2b$ values according to the well-known formulas $\rho_{2p_y} = c_{2p_y}{}^2 = 2b/B^o$ and $\rho_{2p_x} = c_{2p_x}{}^2 = 2a/B^o$. The isotropic Fermi contact term, 6.86 G, has to be compared with the atomic nitrogen isotropic hyperfine constant, $A^o_{iso} = 646.2$ G. In this case one has $\rho_{2s} = c_{2s}{}^2 = a_{iso}/A^o_{iso} = 0.0106$. This small value is, as usual, composed of two distinct parts, the first one due to a direct contribution of the nitrogen 2s orbital to the SOMO and the second to the spin polarization of the ns orbitals by the unpaired electron localized on the orthogonal π_y orbital. The total spin density on the N atom of the adsorbed NO(a) species is thus $\rho(N)_{total} = \rho(2p_x) + \rho(2p_y) + \rho(2s) = 0.803$. This result, with a remarkable localization of the spin density on the N atom, is not surprising taking into account the prevalent nitrogen character of the antibonding orbitals in NO. The detailed results of the spin density analysis for adsorbed NO(a) are listed in Table 2. The spin density on the other two species is expected to be similar.

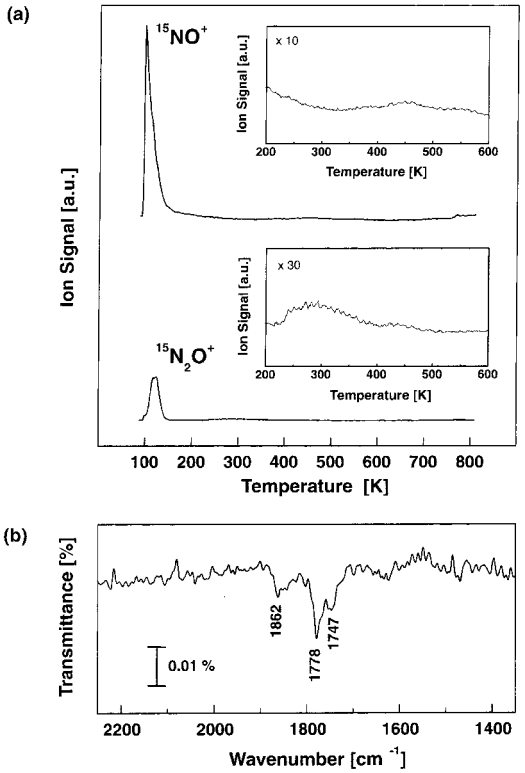

Figure 4. (a) TDS spectra after NO exposure of 5 L at 90 K. Shown are the spectra for $^{15}NO^+$ and $^{15}N_2O^+$. The upper inset shows the amplified $^{15}NO^+$ signal in the temperature range between 200 and 600 K. The lower inset shows the amplified $^{15}N_2O^+$ signal in the temperature range between 200 and 600 K. (b) FTIR spectra of ^{15}NO taken at 90 K for an exposure of 5 L.

3.2. NO Adsorption on MgO Thin Films. MgO ultrathin films grown on a Mo(100) substrate have been exposed to NO in a UHV chamber. Figure 4a (upper spectrum) shows the TDS

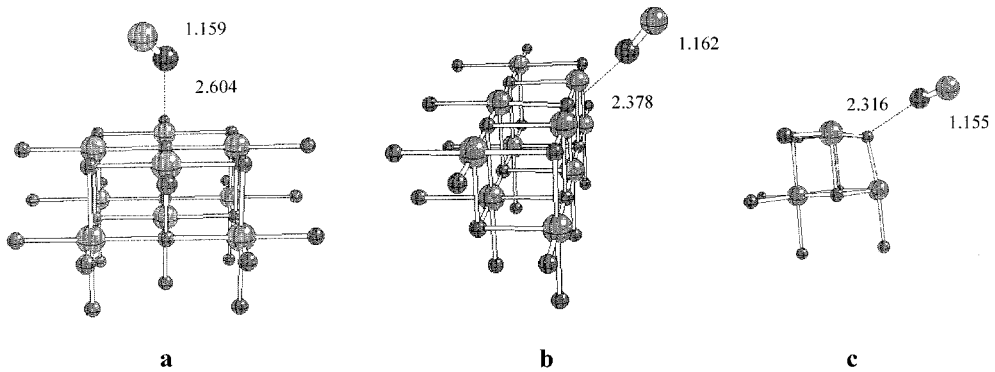

Figure 5. Structure of NO physisorbed on the Mg^{2+} cations of the MgO(100) surface. (a) Terrace ($Mg_9O_9ECP_{17}$); (b) edge ($Mg_{10}O_{10}ECP_{12}$); (c) corner ($Mg_4O_4ECP_6$). Small spheres: Mg; large spheres: O; black sphere: N. Distances are in angstroms.

TABLE 3: Experimental IR Frequencies (cm^{-1}) for NO and $(NO)_2$ Adsorbed on MgO Thin Films and Polycrystals[a]

this work			ref 5		
assign.	$\omega(^{15}NO)^b$	$\Delta\omega(^{14}NO)$	assign.	$\omega(^{14}NO)$	$\Delta\omega(^{14}NO)$
$\nu_s(NO)_2$	1862 (1896)	+20	$\nu_s(NO)_2$	1896	+20
$\nu_{as}(NO)_2$	(c)		$\nu_s(NO)_2$	1866	−10
ν(NO)	1778 (1810)	−66	$\nu_{as}(NO)_2$	1810	−66
ν(NO)	1747 (1779)	−97	$\nu_{as}(NO)_2$	1745	−130

[a] Experimental values for gas-phase or matrix-isolated molecules: ^{14}NO 1876 cm^{-1},[49] ^{15}NO 1839 cm^{-1},[49] $^{14}(NO)_2$ ν_s 1866 cm^{-1}, ν_{as} 1780 cm^{-1}.[56] [b] Scaled values for ^{14}NO in parentheses. [c] Not observed because of surface normal dipole selection rule.

results after exposing the sample to 5 Langmuir of ^{15}NO at 95 K. *m*/*z* of 31 and 46 amu are shown as a function of the sample temperature. A narrow peak for $m/z = 31$ amu is detected with maximum desorption rate at 100 K. A small reproducible shoulder can be observed at 120 K. In addition, a small desorption signal is observed at 450 K (inset of Figure 4a). The desorption at 100 K is attributed to physisorbed ^{15}NO and the desorption at 450 K results from chemisorbed ^{15}NO species on defects such as F centers.[47] The shoulder at 120 K is attributed to a part of the fragmentation pattern of $^{15}N_2O$, which forms at the surface and desorbs at 120 K as shown in Figure 4a (lower spectrum). This species also desorbs at around 280 K (see inset Figure 4a). These results are in qualitative agreement with those obtained by the group of Goodman[48] with the difference that on our films considerably less N_2O is formed.

At the same ^{15}NO exposures FTIR spectra were recorded at 95 K. Three bands at 1862, 1778, and 1741 cm^{-1} are observed in Figure 4b. After annealing the sample to 150 K they completely disappear. If we take into account the isotope effect, 34 cm^{-1}, and refer our values to ^{14}NO, the bands are at 1896, 1810, and 1779 cm^{-1}, respectively, Table 3. We note that the absorption bands in Figure 4 are very small with respect to the amount of absorbed NO. This indicates that the axis of the NO molecule is tilted with respect to the surface normal. In both cases one component of the spectrum is blue-shifted with respect to free NO (free molecule exp. frequency, $\omega_e = 1876$ cm^{-1}; the harmonic frequency, ω_0, is estimated to be 1904 cm^{-1}).[49] The frequencies of these bands are close to those obtained by Zecchina et al.[5] for the adsorption of NO on MgO microcrystals, see Table 3. According to Zecchina et al.[5] the spectrum obtained for NO on MgO powders is the superposition of two pairs of bands assigned to *cis*-$(NO)_2$ species, adsorbed on two different surface sites. Each pair of bands is due to the symmetric and the antisymmetric stretching modes of $(NO)_2$. Therefore we assign the blue shifted band (1862 cm^{-1}) to the symmetric stretch mode of $(NO)_2$. In our case the antisymmetric stretch mode of the dimer is not visible due to the surface normal selection rule. Thus the vibrational bands at 1778 and 1747 cm^{-1} are related to the NO monomers adsorbed on the defect sites.

Another feature which is revealed by the TDS experiment is the formation of $^{15}N_2O$ pointing toward the presence of reactive sites on the MgO thin films. In this context, it is interesting to investigate whether surface oxygen is involved in any reaction path. For this $Mg^{18}O$ films were produced by evaporating Mg in $^{18}O_2$ background (5×10^{-7} mbar). If the MgO surface is involved ^{18}O-containing species should be detected. No such species could be observed in our TDS experiments.

3.3. Quantum Chemical Calculations. In this section we report only the energetic and structural data from the quantum calculations leaving the discussion of the computed observable properties to the following section. We have considered the adsorption of NO on various sites of the MgO surface (terrace, edge, step, and corner sites). On each of these sites NO can interact with the N- or the O-ends with a surface anion or cation or with both. This gives rise in principle to a large number of possible adsorption modes. It is well-known that the CO molecule binds at the terrace sites of MgO with the C-end pointing down toward a surface Mg^{2+} ion and that O-down CO is less favorable.[50] Also for NO the O-down orientation is unfavorable as suggested by some authors[10] and confirmed by our calculations. We thus considered first NO adsorbed with N at metal cations at the MgO(100) terrace sites. The geometry optimization leads to a minimum where the molecule is 2.60 Å from the surface with a N−O distance which is virtually identical to that of the free molecule, Figure 5a. The binding energy is 0.1 eV before correction by the BSSE and ≈0 eV after. A similar structure and binding energy have been reported also by Lu et al.[10] The adsorption energy is certainly underestimated because of the poor description of dispersion forces in DFT. In fact, this is the reason theoretical calculations predict too small bindings for CO on MgO (0.04 eV instead of the experimental value of 0.14 eV).[51] On the Mg^{2+} sites NO is interacting only with one Mg^{2+} cation with the NO axis tilted from the surface normal, Figure 5a. Physisorbed NO is found also on low-coordinated cations at edges, Figure 5b, and corners, Figure 5c, with slightly larger interaction energies because of the increasing strength of the electric field, Table 4. The molecule is virtually unperturbed with respect to free NO.

In a second bonding mode, the NO molecule interacts primarily with surface O^{2-} anions. On the terrace sites, NO in this bonding mode is at 2.35 Å from the O^{2-} anion with the NO axis tilted with respect to the surface normal, Figure 6a. The molecule is weakly bound by 0.11 eV (after BSSE), Table 4. This mode has not been reported before by other authors for

TABLE 4: Electronic Properties of Physisorbed and Chemisorbed NO Monomers on Various Sites of the MgO Surface (DFT-B3LYP results)

system	figure	D_e (eV)[a]	r(NO) Å	a_{iso} (G)	2B (G)	Δ (eV)[b]	Δω (cm^{-1})[c]
free NO			1.159	6.2	26.0		
Physisorbed NO on Mg^{2+} Cations							
terrace	5a	0.0	1.159	5.8	25.3	0.19 (0.11)	−29
edge	5b	0.13	1.162	6.5	25.0	0.34 (0.21)	−67
corner	5c	0.20	1.155	6.8	24.3	0.10 (0.09)	−11
expt				6.86	27.2	0.075	
Adsorbed NO on O^{2-} Anions (metastable)							
terrace	6a	0.11	1.175	5.4	24.1	0.66 (0.50)	−149
edge 1	6b	0.30	1.183	6.5	22.6	1.26 (1.06)	−189
edge 2	6c	0.31	1.174	6.9	22.1	1.01 (0.82)	−143
corner	6d	0.55	1.199	7.6	28.9	>1	−280
Chemisorbed NO on O^{2-} Anions							
edge 1	7a	0.31	1.284	11.7	25.5		−618
step	7b	0.47	1.280	12.3	24.9		−597
edge 2	7c	0.24	1.272	10.4	26.0		−586
corner	7d	0.82	1.307	12.1	26.4		−694

[a] Values corrected by the BSSE. [b] Splitting of NO π_x and π_y levels (HF values in parentheses). [c] Computed $\omega_0 = 1982$ cm^{-1}.

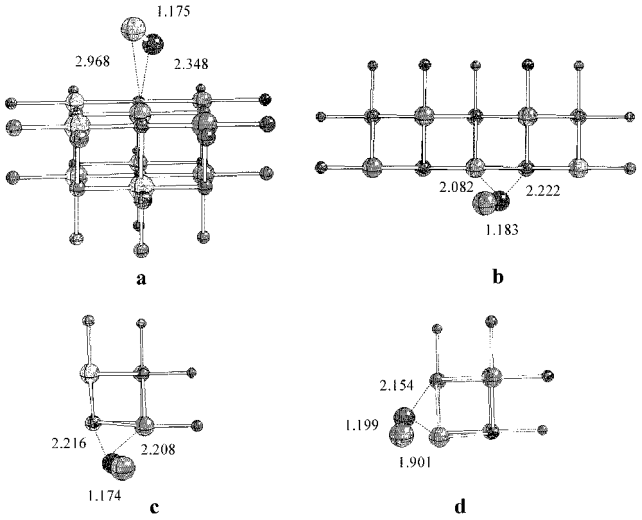

Figure 6. Structure of NO adsorbed on the O^{2-} anions of the MgO-(100) surface. (a) Terrace (Mg_9O_9 ECP_{17}); (b) edge 1 ($Mg_{10}O_{10}ECP_{12}$); (c) edge 2 ($Mg_4O_4ECP_6$); (d) corner ($Mg_4O_4ECP_6$). Small spheres: Mg; large spheres: O; black sphere: N. Distances are in angstroms.

MgO,[10] but it is stable on CaO.[14] NO is more strongly bound at low-coordinated anions where the N-end is actually in a bridge position between O^{2-} and Mg^{2+}. We found two distinct minima, characterized by different geometrical parameters. We denote the first one as metastable NO and the second one as chemisorbed NO, Figure 6b-d and 7a−d. On four-coordinated O sites (edge 1 or edge 2 models, Figures 6b and 6c), the bond of metastable NO is of ≈0.3 eV. The N−O bond length is slightly elongated with respect to the gas phase, by 0.01−0.02 Å, indicating the formation of a weak covalent bond with the surface. If the interaction involves three-coordinated O sites the interaction is even stronger, up to 0.5 eV, and the distortion more pronounced, see Figure 6d and Table 4. This bonding mode is thus intermediate between "physisorbed" and "chemisorbed"; it can be considered as a precursor state of chemisorbed NO. This latter is characterized by a much shorter surface−NO distance and by an elongated N−O bond, Figure 7a−d. Notice that chemisorbed NO does not form on terrace sites but only on low-coordinated oxygen sites. This is in agreement with the EPR experiments which show that only 2% of the

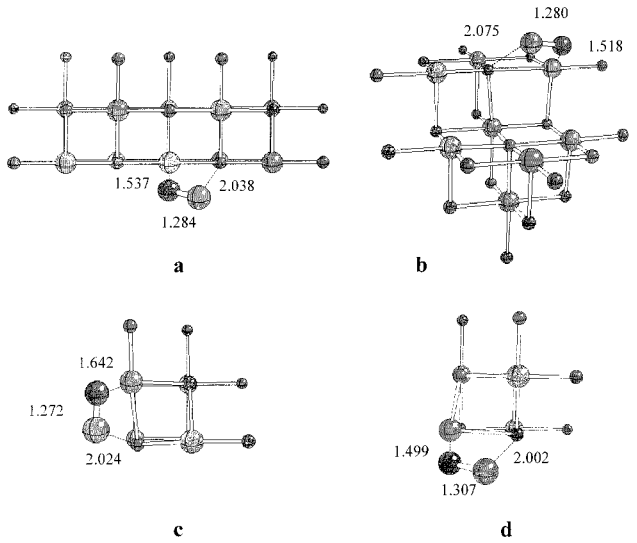

Figure 7. Structure of NO chemisorbed on O^{2-} anions of the MgO-(100) surface. (a) Edge 1 ($Mg_4O_4ECP_{12}$); (b) step ($Mg_8O_8ECP_{12}$); (c) edge 2 ($Mg_4O_4ECP_6$); (d) corner ($Mg_4O_4ECP_6$). Small spheres: Mg; large spheres: O; black sphere: N. Distances are in angstroms.

paramagnetic species form a chemisorbed surface complex, the rest being of "physisorbed" nature. In chemisorbed NO, the N atom interacts with a surface O anion with a bond length of 1.5−1.6 Å and the molecule is almost "parallel" to the surface, with the O-end interacting electrostatically with a surface cation, Figure 7. This bonding mode can be also described as a surface $(NO_2)^{2-}$ species. On low-coordinated sites, like a corner, chemisorbed NO is bound by up to 0.8 eV, Table 4. Somewhat larger binding energies have been reported for these species by Lu et al.[10] The two minima corresponding to metastable and chemisorbed forms of NO on O anions must be separated by a small energy barrier (not investigate here). The metastable precursor has not been seen in EPR. Given the very small amount of sites involved, these species probably cannot be detected at low temperature where the spectrum is dominated by NO physisorbed on cations. On the other hand, the increase in temperature required to desorb physisorbed NO will probably result in the transformation of the metastable precursor into the chemisorbed species stable at RT.

Finally, we have considered the stability of a $(NO)_2$ dimer on the terrace sites of MgO(100). In gas-phase, $(NO)_2$ is very weakly bound, ≈0.1 eV.[52] The most stable form is *cis*-$(NO)_2$ with *trans*-$(NO)_2$ slightly higher in energy.[53] The theoretical calculations show a relatively long N−N distance. On the surface only the cis form is expected. The geometry optimization shows the formation of a stable *cis*-$(NO)_2$ complex bound at metal cations, characterized by a short N−N distance, 1.81 Å, Figure 8, and by an adsorption energy of 0.08 eV (BSSE corrected; computed as $E[(NO)_2/MgO] - E(MgO) - 2E(NO)$). A similar structure and stability for NO dimers on MgO has been reported by Lu et al.[10] No stable structure of the $(NO)_2$ dimer has been found on the oxide anions. This result shows that on the terrace sites the formation of the $(NO)_2$ dimer can compete with that of NO monomers. Thus, only diamagnetic species are expected to form on the MgO terraces, while paramagnetic NO molecules are expected to decorate the low-coordination cations where the bond strength is higher and dominates over dimer formation. It should be mentioned that recently it has been shown that gas-phase $X^-(NO)_2$ complexes (X = Cl or I) are stable thanks to the occurrence of charge transfer from the X^- anion to the lowest unoccupied level of $(NO)_2$.[54] In principle, this suggests that although $(NO)_2$ dimers

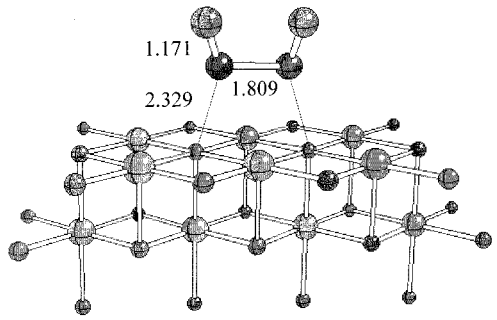

Figure 8. Structure of $(NO)_2$ dimer adsorbed on the terrace sites of the MgO(100) surface ($Mg_{10}O_{10}ECP_{16}$). Small spheres: Mg; large spheres: O; black sphere: N. Distances are in angstroms.

do not form on oxide anions at terraces they could be stabilized at low-coordinated O^{2-} anions, e.g., at a corner site. In any case, the existence of weakly bound $(NO)_2$ dimers is consistent with the TDS spectra as the desorption of the dimer around 100 K results in its dissociation into gas-phase monomers.

4. Discussion

The EPR data show that only ≈0.5% of the surface is covered by NO adsorbed in radical form, the rest being diamagnetic. Two different paramagnetic forms of adsorbed NO are identified at the surface of MgO. The first one (chemisorbed species) is a radical anion having $(NO_2)^{2-}$ formula and is formed in very small amounts by reaction of NO with a particularly active O^{2-} surface oxide ion according to the following equation:

$$NO_g + O^{2-}{}_{surf} \rightarrow (NO_2)^{2-}{}_{surf} \qquad (10)$$

This species is irreversibly formed at RT and is not removable upon simple outgassing at RT. The amount of $(NO_2)^{2-}$ formed at the surface is about 2% of all paramagnetic species derived from NO (Table 1). The second paramagnetic form is constituted by neutral isolated molecules adsorbed at three specific sites of the surface of MgO. These species (physisorbed NO) are much more abundant than the $(NO_2)^{2-}$ radical anions and represent about the 98% of the total. The interaction of NO with the surface electric field causes a weak polarization of the molecule leading to a small orbital rearrangement monitored in terms of the energy splitting Δ between the π antibonding orbitals. Three well distinct Δ values are characteristic of three different sites. The three sites have different abundance at the surface and the reported relative amounts, Table 1, are well reproducible along with a number of experiments on different samples. NO is therefore a suitable molecular probe for specific sites of the surface which are particularly interesting as they are highly active and are also involved in the dissociative chemisorption of the hydrogen molecule.[55]

The TDS spectra of NO adsorbed on MgO thin films show a major peak at 100 K which is attributed to the desorption of residual NO dimers from five-coordinated terrace sites and monomers from defect sites. A small peak at 450 K is due to chemisorbed NO. On single crystals, a major peak in the TDS spectrum has been found at 84 K with a shoulder at 100 K.[2,3] Similar values have been reported for NO on MgO(100) films by Rodriguez et al.[13] who assigned a broad feature at 140 K to NO adsorption at imperfections (≈0.2 ML).

We can try to summarize the TDS and EPR data and to combine them with our calculations. On the terrace sites NO monomers interact very weakly and prefer to form dimers, $(NO)_2$. Only at defect sites (low-coordinated cations) the interaction of NO monomers with the MgO surface is stronger and prevents the formation of the diamagnetic dimers. The small minority of chemisorbed species is formed only at low coordinated anions (steps, edges, or corners) or oxygen vacancies. This picture is fully supported by the analysis of the hfc's and *g*-values and by the FTIR spectra. In Table 4 we report the computed isotropic and dipolar parts of the hyperfine coupling constant for both physisorbed and chemisorbed NO (for the free molecule the computed hfc's are in close agreement with the experiment, with errors of ≈1 G). NO physisorbed on cations exhibits only very small changes in the hyperfine matrix with respect to the free gas-phase molecule, Table 4. This is fully consistent with the EPR spectra which show an a_{iso} value almost identical to that of the free molecule. The computed spin population on N, 0.70 (NO on Mg^{2+} edge site, Figure 5b), is slightly smaller than that estimated from EPR, 0.803, and is mainly localized on a p-type orbital. Another important information about the kind of adsorbed species comes from the splitting of the π orbitals of NO as measured in EPR. In the calculations Δ has been determined as the energy difference between the two electronic configurations $(\pi_x)^1(\pi_y)^0$ and $(\pi_x)^0(\pi_y)^1$ of adsorbed NO (DFT-B3LYP and HF results, Table 4). Δ is smallest for NO physisorbed on cations, 0.1−0.2 eV. The Δ values are in quantitative agreement with the experiment, although some care is necessary in the comparison because of the difficulties in determining this quantity at both theoretical and experimental levels; therefore, one can safely conclude that NO(a), NO(b), and NO(c) in the EPR spectrum correspond to physisorbed NO molecules at differently coordinated cations (terraces, steps, edges, corners), Figure 5, although a more detailed assignment is not possible because the changes in Δ are within the uncertainty of the theoretical calculations.

The FTIR spectra are similar to those obtained on polycrystalline MgO by Escalona-Platero et al.,[5] again confirming that similar adsorption features emerge from the analysis of various forms of the material. So far the interpretation, ref 5, has been based entirely on the formation of $(NO)_2$ dimers, consistent with the previous discussion which confirms the existence of these species. The present study shows that NO monomers are also present on the surface. Calculated vibrational frequencies give a substantial support to the coexistence of NO monomers and dimers. In fact, NO physisorbed on cations is characterized by frequency red-shifts with respect to free NO in the range 10−70 cm^{-1}, Table 4, consistent with the shifts measured for the MgO films, see Table 3.

5. Conclusions

To summarize, the following picture emerges from the analysis of the various experimental and theoretical data on the NO/MgO system:

- The EPR experiments indicate that only 0.5% of adsorbed NO is in paramagnetic form, the rest of the sites being occupied by diamagnetic species. Out of the paramagnetic species, 98% are physisorbed, and only 2% are chemisorbed and stable at RT.
- The TDS on single crystals[2,3] shows a major low-coverage desorption peak at 84 K, which corresponds to the adsorption of NO dimers to the five-coordinated sites. A broad weak desorption feature is observed around 100 K. Thus, on the MgO thin films the immediate desorption of NO at the beginning of the temperature ramp can be interpreted as residual desorption of NO dimers from terrace sites and NO monomers from defect sites.

- A small fraction of N_2O forms at 120 K on the thin films, probably because of the existence of special defect centers chemically more active. Work is in progress to identify these sites.[15]
- The EPR data show that the NO monomers are bound at cation sites (at least three) with different abundances (11%, 32%, and 55%); for all these sites the splitting of the π levels is small (weak interaction and small surface electric field), and the electronic structure and spin distribution are very similar to those of gas-phase NO.
- The FTIR spectra of NO/MgO thin films support the existence of NO dimers on terrace sites and NO monomers adsorbed on the defect sites.
- The quantum chemical calculations show that NO monomers and dimers are very weakly adsorbed on the MgO terraces (either at cations or at anions). Slightly stronger physisorption bonds are found for NO monomers bound at low-coordinated cations. On the low-coordinated O anions NO forms chemisorbed species with stronger bonding. These species, however, are associated to metastable precursor states where the NO molecule is partially activated and the bonding is relatively low. These species have not been detected in EPR. This could be due to the fact that they are a minority of the paramagnetic species and that they convert into the more stable chemisorbed forms by raising the temperature.
- The calculations of the spectral features, hyperfine constants, splitting of NO π levels (Δ), and frequency shifts are consistent with the measured data and reinforce the general interpretation reported above.

In conclusion, at low temperature $(NO)_2$ dimers form on MgO terraces (not detected by EPR), while a small amount of NO monomers forms at low-coordinated cations where the bonding with the defects is larger than the NO−NO one. This allows us to detect and quantify the presence of low-coordinated Mg^{2+} cations on the surface of MgO.

Acknowledgment. We are thankful for the support of the Italian INFM through the PRA-ISADORA project and of the Ministry of University and Research (MURST) through the national program: "Strati ultrasottili di ossidi e solfuri inorganici: crescita, caratterizzazione e reattività superficiale".

References and Notes

(1) *Oxide Surfaces, The Chemical Physics of Solid Surfaces*; Woodruff, P., Ed.; Elsevier: Amsterdam, 2001; Vol. 9.
(2) Wichtendahl, R.; Rodriguez-Rodrigo, R.; Härtel, U.; Kuhlenbeck, H.; Freund, H.-J. *Surf. Sci.* **1999**, *90*, 423.
(3) Wichtendahl, R.; Rodriguez-Rodrigo, R.; Härtel, U.; Kuhlenbeck, H.; Freund, H.-J. *Phys. Stat. Sol. (a)* **1999**, *173*, 93.
(4) Kolmarov, A.; Stultz, J.; Goodman, D. W. *J. Chem. Phys.* **2000**, *113*, 7564.
(5) Escalona Platero, E.; Spoto, G.; Zecchina, A. *J. Chem. Soc., Faraday Trans. 1* **1985**, *81*, 1283.
(6) Escalona Platero, E.; Scarano, D.; Spoto, G.; Zecchina, A. *Faraday Discuss.* **1985**, *80*, 183.
(7) Lunsford, J. H. *J. Chem. Phys.* **1967**, *46*, 4347.
(8) Zhang, G.; Tanaka, T.; Yamaguchi, T.; Hattori, H.; Tanabe, K. *J. Phys. Chem.* **1990**, *94*, 506.
(9) Lu, X.; Xu, X.; Wang, N.; Zhang, Q. *Chem. Phys. Lett.* **1999**, *300*, 109.
(10) Lu, X.; Xu, X.; Wang, N.; Zhang, Q. *J. Phys. Chem. B* **1999**, *103*, 5657.
(11) Yanagisawa, Y.; Kuramoto, K.; Yamabe, S. *J. Phys. Chem. B* **1999**, *103*, 11078.
(12) Rodriguez, J. A.; Jirsak, T.; Kim, J. Y.; Larese, J. S.; Maiti, A. *Chem. Phys. Lett.* **2000**, *330*, 475.
(13) Rodriguez, J. A.; Jirsak, T.; Perez, M.; Gonzales, L.; Maiti, A. *J. Chem. Phys.* **2001**, *114*, 4186.
(14) Snis, A.; Panas, I. *Surf. Sci.* **1998**, *412/413*, 477.
(15) Di Valentin, C.; Pacchioni, G.; Abbet, S.; Heiz, U. To be published.
(16) Knözinger, E.; Jacob, K.-H.; Singh, S.; Hofmann, P. *Surf. Sci.* **1993**, *290*, 388.
(17) Heiz, U.; Vanolli, F.; Trento, L.; Schneider, W.-D. *Rev. Sci. Instrum.* **1997**, *68*, 1986.
(18) Schaffner, M.-H.; Patthey, F.; Schneider, W.-D. *Surf. Sci.* **1998**, *417*, 159.
(19) Wu, M.-C.; Corneille, J. S.; Estrada, C. A.; He, J.-W.; Goodman, D. W. *J. Vac. Sci. Technol. A* **1992**, *10*, 472.
(20) Wu, M.-C.; Corneille, J. S.; Estrada, C. A.; He, J.-W.; Goodman, D. W. *Chem. Phys. Lett.* **1991**, *182*, 472.
(21) Liehr, M.; Thiry, P. A.; Pireaux, J. J.; Caudano, R. *Phys. Rev. B* **1986**, *33*, 5682.
(22) Tjeng, L. H.; Vos, A. R.; Sawatzky, G. A. *Surf. Sci.* **1990**, *235*, 269.
(23) He, J.-W.; Møller, P. L. *Chem. Phys. Lett.* **1986**, *129*, 13.
(24) Nygren, M. A.; Petterson, L. G. M. *J. Chem. Phys.* **1996**, *105*, 9339.
(25) He, J.-W.; Cesar, A. E.; Corneille, J. S.; Wu, M.-C.; Goodman, D. W. *Surf. Sci.* **1992**, *261*, 167.
(26) Abbet, S.; Riedo, E.; Brune, H.; Heiz, U.; Ferrari, A. M.; Giordano, L.; Pacchioni, G. *J. Am. Chem. Soc.* **2001**, *123*, 6172−6178.
(27) Schintke, S.; Messerli, S.; Pivetta, M.; Libioulle, L.; Patthey, F.; Stengel, M.; De Vita, A.; Schneider, W.-D. To be published.
(28) Heiz, U.; Schneider, W.-D. *J. Phys. D: Appl. Phys.* **2000**, *33*, R85.
(29) *Cluster Models for Surface and Bulk Phenomena*, NATO ASI Series B; Pacchioni, G., Bagus, P. S., Parmigiani, F., Eds.; Plenum: New York, 1992; Vol. 283.
(30) Sauer, J.; Ugliengo, P.; Garrone, E.; Saunders, V. R. *Chem. Rev.* **1994**, *94*, 2095.
(31) Pacchioni, G.; Ferrari, A. M.; Marquez, A. M.; Illas, F. *J. Comput. Chem.* **1997**, *18*, 617.
(32) Winter, N. W.; Pitzer, R. M. *J. Chem. Phys.* **1988**, *89*, 446.
(33) Nygren, M. A.; Pettersson, L. G. M.; Barandiaran, Z.; Seijo, L. *J. Chem. Phys.* **1994**, *100*, 2010.
(34) Yudanov, I. V.; Nasluzov, V. A.; Neyman, K. M.; Rösch, N. *Int. J. Quantum Chem.* **1997**, *65*, 975.
(35) *Chemisorption and Reactivity on Supported Clusters and Thin Films*, NATO ASI Series E; Lambert, R. M., Pacchioni, G., Eds.; Kluwer: Dordrecht, 1997; Vol. 331.
(36) Neyman, K. M.; Pacchioni, G.; Rösch, N. In *Recent Development and Applications of Modern Density Functional Theory*; Seminario, J., Ed.; Elsevier: Amsterdam, 1996; Theoretical and Computational Chemistry, Vol. 4., p 569.
(37) Becke, A. D. *J. Chem. Phys.* **1993**, *98*, 5648.
(38) Lee, C.; Yang, W.; Parr, R. G. *Phys. Rev. B* **1988**, *37*, 785.
(39) Ditchfield, R.; Hehre, W. J.; Pople, J. A. *J. Chem. Phys.* **1971**, *54*, 724.
(40) Barone, V. In *Recent Advances in Density Functional Methods*, Part I; Chong, D. P., Ed.; World Scientific: Singapore, 1996.
(41) Boys, S. F.; Bernardi, F. *Mol. Phys.* **1970**, *19*, 553.
(42) Weil, J. A.; Bolton, J. R.; Wertz, J. E. *Electron Paramagnetic Resonance*; John Wiley & Sons: New York, 1994.
(43) Frisch, M. J. et al. *Gaussian 98*; Gaussian Inc.: Pittsburgh, PA, 1997.
(44) Paganini, M. C.; Chiesa, M.; Giamello, E.; Di Valentin, C.; Pacchioni, G. To be published.
(45) Brailsford, J. R.; Morton, J. R.; Vannotti, L. E. *J. Phys. Chem.* **1969**, *50*, 1051.
(46) Känzig, W.; Cohen, M. H. *Phys. Rev. Lett.* **1959**, *3*, 509.
(47) Sanchez, A.; Abbet, S.; Heiz, U.; Schneider, W.-D.; Häkkinen, H.; Barnett, R. N.; Landman, U. *J. Phys. Chem. A* **1999**, *103*, 9573.
(48) Kolmakov, A.; Stultz, J.; Goodman, D. W. *J. Phys. Chem.* **2000**, *113*, 7564.
(49) Huber, K. P.; Herzberg, G. *Molecular Spectra and Molecular Structure, IV Constants of Diatomic Molecules*; Van Nostrand Reinhold: New York, 1979.
(50) Pacchioni, G.; Cogliandro, G.; Bagus, P. S. *Int. J. Quantum Chem.* **1992**, *42*, 1115.
(51) Damin, A.; Dovesi, R.; Zecchina, A.; Ugliengo, P. *Surf. Sci.* **2001**, *479*, 255.
(52) Duarte, H. A.; Proynov, E.; Salahub, D. R. *J. Chem. Phys.* **1998**, *109*, 26.
(53) Dinerman, C. E.; Ewing, G. E. *J. Chem. Phys.* **1970**, *53*, 626.
(54) Hiraoka, K.; Iino, T.; Eguchi, D.; Mizuno, T.; Yamabe, S. *Chem. Phys. Lett.* **2000**, *323*, 155.
(55) Chiesa, M.; Paganini, M. C.; Giamello, E. To be published.
(56) Canty, J. F.; Stone, E. G.; Bach, S. B. H.; Ball, D. W. *Chem. Phys.* **1997**, *216*, 81.